



HAL
open science

A pilot-scale solar reactor for the production of hydrogen and carbon black from methane splitting

Sylvain Rodat, Stéphane Abanades, Jean-Louis Sans, Gilles Flamant

► To cite this version:

Sylvain Rodat, Stéphane Abanades, Jean-Louis Sans, Gilles Flamant. A pilot-scale solar reactor for the production of hydrogen and carbon black from methane splitting. *International Journal of Hydrogen Energy*, 2010, 35 (15), pp.7748-7758. 10.1016/j.ijhydene.2010.05.057 . hal-02567190

HAL Id: hal-02567190

<https://hal.science/hal-02567190>

Submitted on 13 May 2020

HAL is a multi-disciplinary open access archive for the deposit and dissemination of scientific research documents, whether they are published or not. The documents may come from teaching and research institutions in France or abroad, or from public or private research centers.

L'archive ouverte pluridisciplinaire **HAL**, est destinée au dépôt et à la diffusion de documents scientifiques de niveau recherche, publiés ou non, émanant des établissements d'enseignement et de recherche français ou étrangers, des laboratoires publics ou privés.

A pilot-scale solar reactor for the production of hydrogen and carbon black from methane splitting

Sylvain Rodat*, Stéphane Abanades, Jean-Louis Sans and Gilles Flamant

PROMES-CNRS Laboratory, 7 rue du four solaire, 66120 FONT-ROMEUE, France

Abstract

A pilot-scale solar reactor was designed and operated at the 1 MW solar furnace of CNRS for H₂ and carbon black production from methane splitting. This constitutes the final objective of the SOLHYCARB EC project. The reaction of CH₄ dissociation produces H₂ and carbon nanoparticles without CO₂ emissions and with a solar upgrade of 8% of the high heating value of the products. The reactor was composed of 7 tubular reaction zones and of a graphite cavity-type solar receiver behaving as a black-body cavity. Temperature measurements around the cavity showed a homogeneous temperature distribution. The influence of temperature (1608K-1928K) and residence time (37-71 ms) on methane conversion, hydrogen yield, and carbon yield was especially stressed. For 900 g/h of CH₄ injected (50% molar, the rest being argon) at 1800K, this reactor produced 200 g/h H₂ (88% H₂ yield), 330 g/h CB (49% C yield) and 340 g/h C₂H₂ with a thermal efficiency of 15%. C₂H₂ was the most important by-product and its amount decreased by increasing the residence time. A 2D thermal model of the reactor was developed. It showed that the design of the reactor front face

* Corresponding author.
Tel: +33 4 68 30 77 31
Fax: +33 4 68 30 29 40
E-mail address: sylvain.rodatt@promes.cnrs.fr .

could be drastically improved to lower thermal losses. The optimised design could reach 77% of the ideal black-body absorption efficiency (86% at 1800K), i.e. 66%.

Keywords: Hydrogen production; Solar thermal energy; Methane dissociation; Solar reactor; Thermal simulation.

1.Introduction

Solar methane dissociation offers the possibility for the clean co-production of hydrogen and carbon black. The benefits of such a process can be found elsewhere [1-2]. It appears as an alternative to the steam methane reforming and the furnace process [3] dedicated to the conventional production of hydrogen and carbon black, respectively. The solar process avoids both CO₂ emissions from fossil fuel combustion required to carry out the endothermic reaction and from the reaction of steam reforming thus avoiding 13.9 kg-equivalent CO₂/kg H₂ produced as compared to conventional processes [4]. Indeed, the energy supplied by fossil fuel combustion is replaced by concentrated solar energy and methane cracking results in solid carbon and hydrogen only. The theoretical energy balance of the reaction is reported in Figure 1. It shows that the High Heating Value (HHV) of methane is upgraded by solar energy in an amount equal to the enthalpy change of the reaction (76 kJ/mol). Finally, solar energy represents 8% of the HHV of the products, hydrogen 59% and carbon 41%. Anyway, it must be pointed out that the HHV of carbon is lost since it is not destined for energy production but rather for direct industrial application such as tyres or batteries production [5]. Solid carbon could also be an opportunity for a safe carbon storage with a possible future use if ecological situation is favourable [6]. The sensible heat of the products can also be recovered.

Solar chemical reactors devoted to the solar thermal dissociation of methane were proposed at small scale. Maag et al. [7] developed a direct heating solar reactor seeded with particles. A numerical model was also proposed accounting for the unsteady mass and energy conservation equations, coupling convective heat and mass transfers, radiative heat transfer, and chemical kinetics for a two-phase solid–gas flow [8]. Fairly good agreement between the model and the experimental results were obtained. Direct solar heating was also experienced by Kogan et al. [9, 10] with a tornado flow configuration and Hirsch et al. [11]. Indirect heating reactors based on tubular designs were proposed by Dahl et al. [12] and Rodat et al. [13]. Direct heating solar reactors provide better heat transfer to the reaction zone but the window protection against particle deposition is a challenging task. It seems from the current state-of-the-art that indirect heating solar reactors are more mature for scaling up. If the reactor was operated with very high gas velocities (0.3 to 0.8 Mach [5]) and with longer tubes (to keep the same gas residence time), the carbon deposition could be alleviated. The investigation of reaction kinetics was also addressed [14-16]. Reviews on solar methane cracking [17] and catalytic methane decomposition using metal and carbonaceous materials [18] were recently published. Nevertheless, the previous developed reactors do not exceed 10 kW scale. In order to acquire more experience toward a potential industrial application, a 50 kW multi-tubular solar reactor was constructed, tested and simulated in the framework of the European project SOLHYCARB. This 50 kW scale receiver is a step forward in a future industrial application of the process in a solar chemical plant based on a reactor set at the top of a central solar tower receiver and equipped with a secondary concentrator. In the various numerical models previously proposed, special attention was paid to detail the reaction zone. For example, Caliot et al. [19] proposed a model describing the absorption of IR radiations by methane, Kogan et al. [20] published a detailed study on the numerical simulation of their tornado flow configuration, but only few works addressed the global design of an optimised

pilot-scale receiver [7, 21], especially in terms of chemical and thermal reactor efficiencies. This paper presents the experimental chemical performances and energy efficiencies of the pilot-scale solar reactor, and it also focusses on the possible improvements of the receiver predicted by CFD simulations.

2.Experimental set-up

The reactor was designed for a nominal power of 50 kW of incident solar power (Figure 2). The reactor body is made of an aluminium shell (800x780x505 mm) and a water-cooled front face with a 13 cm-diameter aperture to let concentrated solar radiation entering within the reactor cavity. The radiations are absorbed by the graphite cavity (360x400x300 mm) that approaches black-body behaviour. To avoid contact of graphite with the oxidizing atmosphere, the aperture is protected by a domed quartz window (outer diameter of 360 mm) swept by a nitrogen flow. The hemispherical shaped window is advantageous in comparison to a plane window because it is not close to the hot cavity and the focal zone, which avoids window overheating and subsequent irreversible damage. The space between the graphite cavity and the aluminium shell is filled with three different insulating layers to limit conduction losses. It is composed of a 85 mm-thick graphite felt in contact with the cavity ($\lambda=0.53 \text{ W}\cdot\text{m}^{-1}\cdot\text{K}^{-1}$ at 1873K), a 50 mm-thick intermediate refractory ceramic fiber operating up to 1873K (62% Al_2O_3 , 30% SiO_2 , $\lambda=0.35 \text{ W}\cdot\text{m}^{-1}\cdot\text{K}^{-1}$ at 1673K), and a 50 mm-thick outer microporous insulator operating up to 1273K (20% ZrO_2 , 77.5% SiO_2 , 2.5% CaO , $\lambda=0.044 \text{ W}\cdot\text{m}^{-1}\cdot\text{K}^{-1}$ at 1073K). Seven graphite tubes (800 mm length, 26 mm OD, 18 mm ID) cross the graphite cavity horizontally and they are heated both by direct solar radiation and by IR-radiation from the hot graphite cavity walls. In order to maintain the position of the graphite

cavity and to avoid mechanical stress on the tubes, four alumina tubes, positioned vertically as supports at the bottom, hold the graphite cavity.

The experimental equipment is schemed in Figure 3. Each tube is fed with a mixture of argon and methane thanks to two mass-flow controllers dedicated to each tube (total of 14 mass-flow controllers, Brooks Instruments model 5850 S, range 0-10 NL/min for methane and 0-20 NL/min for argon). Each tube entrance is equipped with an absolute pressure sensor. At the exit, the products (particles and gases) from the tubes are collected and cooled down. Then, they are directed toward a filter composed of 6 bags (diameter: 127 mm, length: 1000 mm) enabling the separation of the carbon black from the gaseous phase that is evacuated to the vent. Before this filter, a pump samples a part of the products toward a secondary filter and then to the gas analysis system. This sampling system provides a fast response time of the analysis, since there is no need to wait for the sweeping of the whole volume of the primary filter (about 0.8 m³) to get stable measurements. The gas analysis system is composed of an online analyser for measuring hydrogen and methane concentrations (NGA 2000 MLT3, resolution of 1% of the full scale, range: 0-70% for H₂, 0-10% for CH₄) as well as a gas chromatograph (micro GC Varian CP 4900) for identifying and quantifying the gas species in the course of the experiment. The micro GC is equipped with 2 channels: Channel 1 (MolSieve 5A PLOT 10M Backflush) for H₂, N₂, O₂, CO, CH₄; Channel 2 (PoraPLOT U 10M Backflush) for light hydrocarbons such as CH₄, C₂H₆, C₂H₄, C₂H₂, and H₂. These equipments were previously used during the testing of a 10 kW solar reactor prototype [22].

The control of the temperatures in the reactor is provided by five thermocouples and one solar blind optical pyrometer (wavelength: 5.14 μm) (Figure 4). Two type B thermocouples are set in contact with the graphite cavity, one at the top (B_top), another at the back (B_back). At about the same location, K-thermocouples (K_top and K-back) measure the temperature at 5 cm depth (from the aluminium shell surface) in the insulated zone. In addition, a type B

thermocouple is inserted 24 cm inside the lowest graphite tube on which the optical pyrometer is also pointing, thus giving a redundant temperature measurement of the reaction zone by two different means. A K-thermocouple and a pressure sensor are also positioned on the outlet gas path after the collector.

An experimental run is composed of two steps. The first step is the heating of the reactor under concentrated solar irradiation coming from the 1 MW solar furnace of CNRS-PROMES (the incoming power is regulated thanks to a shutter and to the number of sun-tracking heliostats, 1 MW corresponds to the maximum power of the solar facility with the shutter fully opened and 63 heliostats involved) [22]. During this period, the tubes are fed with pure argon till the targeted temperature is reached. Then, a mixture of argon and methane is injected once the temperature is stabilized and the operating conditions are maintained during about an hour to produce significant amounts of carbon black for further analysis and to be able to analyse the product characteristics with respect to fixed experimental conditions. The cleaning of the filter is realised with air back pulses and carbon is collected at the bottom of the filter at the end of the experiment. The whole experimental installation in operation is shown in Figure 5.

3.Experimental conditions

The experimental conditions are listed in Table 1. Methane mole fractions in the feed range from 25 to 50% in order to maintain sufficient dilution. The main results are recapped in Table 2. After each experimental run at given operating conditions (temperature, pressure and gas flow-rates fixed), the carbon was recovered in the filter so that carbon black samples were representative of specific conditions. About 100 g of sample was recovered after each run and

was available for analysis and characterization. The specific work devoted to the analysis of the carbon black properties is not presented in the following.

4.Results and discussion

4.1.Experimental results

Figure 6 displays typical temperature measurements, H₂ and CH₄ off-gas mole fractions, DNI (Direct Normal Irradiation) recorded for the experimental run #2. It can be decomposed in three experimental stages: heating of the reactor in Ar, cracking period (methane injection), and passive cooling of the reactor (no solar irradiation).

After a heating period of about 40 min under an argon flow in the tubes, the temperature of the reactor reaches 1700K. All the temperature sensors tend to indicate the same mean temperature in the range 1670K-1720K. The highest temperature is given by the pyrometer that points directly on the outer wall of a tube. At about the end of the experiments, the highest temperature is given by the thermocouple called B_{back} but its value is still very close to the one given by the pyrometer. It can be stated that the temperature is homogeneous around the cavity during the methane splitting period. The lowest temperature is given by the thermocouple inserted in a tube (B_{tube}) because it is cooled by the fresh reactants and by the endothermic reaction. During the heating period it can be noted that the temperature measurements are in the following order: Pyrometer > B_{tube} > B_{back} > B_{top} and the opposite ranking is observed during the passive cooling period. Small temperature variations can be observed at the beginning of the injection period, which can be correlated with a decrease of the DNI due to a cloud shadow on the heliostat field. However, it was possible to maintain the temperature around the targeted value by increasing the incoming power

(increased shutter aperture). Concerning the K-thermocouples, they never reach a stable value during the injection period, which means that the insulation layers does not reach thermal steady state. The temperature even increases after the end of the reactor heating due to low thermal conduction and thermal inertia.

When the targeted temperature is reached and stabilized, 31.5 NL/min argon and 10.5 NL/min methane are injected. H_2 is rapidly detected at the exit along with residual CH_4 (not dissociated). The temperature variations impact directly H_2 and CH_4 mole fractions, i.e. a temperature increase results in the H_2 mole fraction increase and vice versa. Since the higher the temperature, the better the conversion, the trend is reverse for the CH_4 mole fraction. Indeed, it decreases when the temperature increases. No continuous analysis of C_2H_2 in the off gas was available but the C_2H_2 mole fraction was rather constant: the chromatography analysis gave a 0.043 mean mole fraction. This value tended to decrease at the end of the injection period, which must be related to the H_2 mole fraction increase and the CH_4 mole fraction decrease. After 2400 s of experiment at constant temperature, the H_2 mole fraction in the off-gas increases slightly as a result of tubes clogging. Carbon deposit in the tubes causes a pressure increase and thereby a residence time increase that favours better CH_4 and C_2H_2 dissociation. After about one hour of methane injection, the methane flow-meters are successively stopped because of the progressive tube blocking.

The reactor performances are given in terms of methane conversion, hydrogen yield, and carbon yield [13]. These parameters pertinently express the performances of the process giving the quantity of methane that has been transformed in the form of hydrogen and carbon, the two targeted products.

- The CH_4 conversion gives the proportion of methane that has been dissociated and it is defined as:

$$X_{CH_4} = \frac{F_{0,CH_4} - F \cdot y_{CH_4}}{F_{0,CH_4}} \quad (1)$$

- The H₂ yield is the proportion of methane that has been converted into hydrogen and it is calculated from:

$$Y_{H_2} = \frac{F \cdot y_{H_2}}{2 \cdot F_{0,CH_4}} \quad (2)$$

- The C yield is the proportion of methane that has been converted into solid carbon and it is expressed as:

$$Y_C = \frac{F_{0,CH_4} - (F \cdot y_{CH_4} + 2 \cdot F \cdot y_{C_2H_2} + 2 \cdot F \cdot y_{C_2H_4} + 2 \cdot F \cdot y_{C_2H_6})}{F_{0,CH_4}} \quad (3)$$

where F_{0,CH_4} is the inlet molar flow-rate of CH₄, y_i is the mole fraction of species i , and F is the total outlet gas flow-rate (including argon as buffer gas) obtained from:

$$F = \frac{F_{Ar}}{1 - (y_{CH_4} + y_{H_2} + y_{C_2H_2} + y_{C_2H_4} + y_{C_2H_6})} \quad (4)$$

F_{Ar} is the molar flow-rate of Ar. In equations (3) and (4), polycyclic aromatic hydrocarbons (PAH) are neglected.

Figure 7 reports the results concerning the first experimental series (Ar: 31.5 NL/min, CH₄: 10.5 NL/min) in terms of methane conversion, hydrogen yield, and carbon yield with increasing temperatures (1608K-1928K). The higher the temperature, the better the chemical performance criteria. Moreover, the CH₄ conversion is always higher than the H₂ yield and

the C yield. This is because the methane dissociation is not complete: a part of the methane is not converted and another part is converted into other C₂ hydrocarbons (mainly C₂H₂). Since the conversion of CH₄ into C₂H₂ leads to the production of 1.5 mole of H₂ per mole of CH₄ without carbon production, the H₂ yield is higher than the C yield. The intermediate C₂H₂ mainly affects the carbon yield. For temperatures above 1778K, complete methane conversion is achieved. It can also be noticed that similar runs lead to close results (runs 3 and 4).

Figure 8 reports the results related to the second experimental series (Ar: 49 NL/min, CH₄: 21 NL/min) in the temperature range 1698K-1873K. Similar trends are observed for the temperature influence but the CH₄ conversion never reaches completion even for temperatures up to 1873K as a result of the higher flow-rates compared to the ones of the first series. For the run #7 (50% of CH₄ in the feed), better chemical performances are obtained due to a higher residence time as a result of the lower argon dilution (Ar: 21 NL/min instead of 49 NL/min). The comparison between the results of the first and second series shows better performances for the first series, which points out again the strong influence of the residence time. Residence time and temperature thus appear as the most critical parameters.

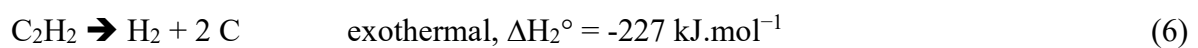
4.2.Kinetic analysis

The kinetic parameters of the global reaction of CH₄ dissociation were estimated on the basis of an isothermal plug-flow reactor model that is described by [23]. A first order kinetic expression following an Arrhenius law was assumed, as proposed by Trommer et al. [23]. The first series was considered since it shows the widest temperature range for a given gas flow-rate. An activation energy of 196 (+/-17) kJ/mol and a pre-exponential factor in the range $1.57 \times 10^7 \text{ s}^{-1}$ - $1.61 \times 10^8 \text{ s}^{-1}$ (accounting for the fit uncertainty) were identified. These values are in agreement with the ones obtained in a previous work on a 10 kW solar reactor [13,22].

An activation energy in the range 172-205 kJ/mol and a frequency factor between $1.42 \times 10^7 \text{ s}^{-1}$ and $1.47 \times 10^8 \text{ s}^{-1}$ were obtained. This result highlights a weak dependency of the kinetics on the two different reactor designs (10 and 50 kW solar reactors). It is also consistent with the reported activation energies for heterogeneous (catalytic) methane decomposition reaction, which vary between 147 kJ/mol for activated carbons as particle loading [23] and 236 kJ/mol for carbon black based catalysts [24].

4.3. Energy efficiencies

The global reaction of direct methane decomposition is not able to predict the formation of C_2H_2 intermediate and a 2-step reaction mechanism was rather considered (Eq. (5) and (6)) to quantify realistic chemical energies associated with the formation of the main products (C, H_2 , and C_2H_2). In order to assess the performances of the reactor with respect to energy conversion efficiency, calorimetric measurements were performed at the cavity entrance (see Figure 4). Thus, the power reaching the back of the water-cooled front face was measured, which allowed the evaluation of the reactor thermochemical and thermal efficiencies, for the following two-step reaction mechanism:



The corresponding thermochemical and thermal efficiencies can be expressed as follows:

$$\eta_{ch} = \frac{F_{0,\text{CH}_4} \cdot X \cdot \int_{T_0}^{T_{\text{reactor}}} C_{p\text{CH}_4} \cdot dT + F_{0,\text{CH}_4} \cdot X \cdot \Delta H_1(T_{\text{reactor}}) + 1/2 \cdot F_{0,\text{CH}_4} \cdot X \cdot Y \cdot \Delta H_2(T_{\text{reactor}})}{P_{\text{solar}}} \quad (7)$$

$$\eta_{th} = \frac{F_{0,CH_4} \int_{T_0}^{T_{reactor}} C_{p_{CH_4}} dT + F_{0,CH_4} X \cdot \Delta H_1(T_{reactor}) + 1/2 \cdot F_{0,CH_4} X \cdot Y \cdot \Delta H_2(T_{reactor}) + F_{Ar} \int_{T_0}^{T_{reactor}} C_{p_{Ar}} dT}{P_{solar}} \quad (8)$$

Where Y is the fractional conversion of reaction (6) defined as $Y = F_{H_2}/F_{0,C_2H_2}$ (F_{0,C_2H_2} is the molar flow-rate of acetylene issued from reaction (5)). X is the fractional conversion of reaction (5). P_{solar} is the solar power input at the cavity entrance (W), C_{p_i} is the specific heat of species i ($J \cdot mol^{-1} \cdot K^{-1}$, function of temperature).

The incoming power varied between 23 and 37 kW (corresponding to mean flux densities between 1.7 and 2.8 MW/m²) depending on the reactor temperature (Figure 9). The resulting efficiencies are reported in Figure 10 for all the experimental runs. The two series can easily be identified. The first one shows lower efficiencies than the second one. This is due to the higher feed gas flow-rates for the second series, which led to higher thermal power conversion. In every cases, the thermochemical efficiency is smaller than the thermal efficiency because the latter accounts for the heating of argon and non converted methane. The highest thermochemical and thermal efficiencies reported (13.5% and 15.2%, respectively) are achieved for the run #7, with 21 NL/min CH₄ and Ar. As a result of a 50% limited dilution, the discrepancy between thermochemical and thermal efficiencies is lower than the one observed for the other runs that correspond to higher argon dilution (70 to 75%). On the basis of run #7, the production at pilot-scale is 200 g/h H₂ (88% H₂ yield), 330 g/h CB (49% C yield), and 340 g/h C₂H₂. The production of C₂H₂ is significant and it could be either recovered as a valuable by-product or further dissociated provided that the residence time is increased.

5. Thermal simulation of the solar cavity receiver

A numerical model was proposed in order to identify and classify the main thermal losses associated with the design of the reactor. A global 2D axisymmetric model of the reactor was created with the commercial software Fluent (12.0.16). In order to get fast convergence and flexibility of the model, the reaction was simulated by a heat sink in the volume of the graphite cavity, which simplifies the tubular zones while taking into account the endothermic reaction. The mesh was created with Gambit (2.4.6) to simulate the whole receiver and to optimise its design. First, the reactor was simulated for comparison with a real experimental run. Then, a new design was proposed for a potential industrial up-scaled application.

The mesh (Figure 11) shows the 2D axisymmetric geometry that approaches the real 3D configuration. The thickness of the insulating layers is respected. However, the reactor is simulated as a cylindrical receiver. Moreover, although the model does not account for the tubes inside the cavity, the related thermal conduction losses are simulated by an equivalent quantity of matter around the outlet pipe that is cooled at the exit. The hemispherical window is not included, the diffuse solar irradiation is directly emitted by a transparent window at the reactor aperture (or at the reactor entrance depending on the case). The Discrete Ordinate model is used to solve the radiative transfer equation. The graphite cavity approaches an ideal blackbody, consequently the emissivity and diffuse fraction are set to 1. Perfectly diffused walls are thus assumed. The N₂ sweeping gas flow-rate is kept constant (24 NL/min). A sensitivity study on the mesh was carried out in order to check independence of the results on the mesh size. A mesh composed of 21000 cells was chosen (element: quad, type: pave) with a smoother definition where the discrete ordinate model is solved to take into account the radiative heat transfer precisely. The convective heat transfer coefficient around the aluminium shell is set to 10 W/m²K. The top left corner of the cavity serves as the reference point for the cavity temperature.

First, the reactor was simulated for a given experimental condition (run #7: Ar and CH₄ flow-rates of 21 NL/min at 1798K). For this experiment, the thermal power required to heat the feed and carry out the two-step reaction was 4316 W. Calorimetric measurements showed that the power reaching the cavity entrance (see Figure 11) was 28.4 kW. Thus the reactor was modelled with this incident solar power. The influence of the heat sink on the cavity temperature was studied (Figure 12). Obviously, increasing the heat sink results in the cavity temperature decrease. For a heat sink of 4316 W, the cavity temperature is still 2020K. Calorimetric measurements were carried out at the cavity entrance for reasons of experimental implementation. The power at the aperture was different due the water-cooled front-face thickness. The model was thus used to estimate the power required at the aperture. To reach the same cavity temperature of 2020K, a power of 53 kW was required at the aperture (as compared to the 28.4 kW required at the cavity entrance, see Figure 11), which points out the high thermal losses due to the thickness of the water-cooled front face (35 mm). The corresponding flux density is 4.14 MW/m². Anyway, this predicted cavity temperature is about 200K higher than the experimentally measured value (about 1800K). This can be explained by additional thermal losses in the real configuration through the sighting portholes devoted to pyrometry measurements and other thermal bridges such as the alumina supports of the graphite cavity. It was shown previously that the reactor insulating layers are not at steady state whereas the simulation is steady, so the transient heat demand also contributes to extra thermal losses. In addition, the approximation of the geometry assumed cylindrical, which especially leads to a smaller water-cooled front face, may explain the discrepancy that corresponds to an additional heat sink of 6 kW (Figure 12).

In the following, these additional thermal losses were neglected since they can be avoided. The thermal sink was thus considered to be directly connected to the thermal power required to heat the feed and carry out the two-step reaction mechanism. Consequently, the possible

maximum heat sink was 10.3 kW (Figure 12) for maintaining the temperature at about 1800K (mean temperature measured experimentally) with 53 kW entering at the aperture. Thus, the thermal efficiency of the reactor was determined to be 19% if the whole heat sink is devoted to the reactants heating and the reaction enthalpy.

The main heat losses were identified to be at the water-cooled front face (66%) and at the aperture (9%). To diminish the heat losses at the aperture, higher solar concentration ratio should be used, but this requires a highly efficient solar concentrating system (capable to provide concentrated solar flux over 4.14 MW/m²). Since the most important thermal losses concern the front face, an optimisation of this component is proposed. It could be better insulated assuming the design represented in Figure 13. The boundaries are the same as for the previous design, but the front face is better insulated and includes a secondary concentrator shape (nevertheless, the aperture diameter is kept the same as in Figure 11). The compound parabolic concentrator (CPC) requires a specifically designed concentrating system as a function of its aperture angle. The CPC is water-cooled and its temperature is fixed at 300K. For 53 kW entering power at the aperture, a temperature of 1800K is obtained for a heat sink of 35 kW, resulting in a thermal efficiency of 66%. In addition, a homogeneous temperature of graphite is obtained. This specific design of the front face permits to increase drastically the thermal efficiency of the reactor. For comparison, the absorption efficiency of a perfectly insulated black-body cavity at 1800K irradiated through the same aperture with 53 kW is 86% according to the following expression [25]:

$$\eta_{Absorption} = 1 - \frac{Q_{Radiation}}{Q_{Reactor}} = 1 - \frac{\sigma(T_{Cavity}^4 - T_0^4)}{DNI.C} \quad (9)$$

with σ , the Stephan Boltzmann constant ($5.67 \cdot 10^{-8} \text{ W} \cdot \text{m}^{-2} \cdot \text{K}^{-4}$), T_{cavity} , the cavity temperature and $T_0 = 298.15 \text{ K}$.

Accordingly, the optimised design reaches 77% of the ideal black-body cavity absorption efficiency. If all the power can be transferred to the reactants, this could result in the production of 1.6 kg/h H₂, 2.7 kg/h CB and 2.8 kg/h C₂H₂ (from Eq. 8 with a thermal efficiency of 66%) assuming similar chemical performances as the ones obtained with 21 NL/min CH₄ and 21 NL/min Ar at 1798K (run #7). Such theoretical production corresponds to about 8 times the experimental production.

6. Conclusion

A pilot-scale solar reactor was tested to turn methane into hydrogen and carbon. For the investigated experimental conditions, CH₄ conversions between 72% and 100% and H₂ yields in the range 57%-88% were reached. Anyway, the carbon yield never exceeded 63%. Thermochemical and thermal efficiencies up to 13.5% and 15.2% were achieved, respectively. In spite of a relatively low carbon yield due to the production of significant amounts of C₂H₂, representative quantities of carbon black were recovered for further characterisation. The carbon black samples must be analysed in order to bring into light correlations between experimental conditions and carbon black properties.

Thermal simulation of the cavity receiver was proposed to evaluate its thermal behaviour. Results showed that 66% of the incoming power was lost through the water-cooled front face as a result of the high temperature gradient between the isothermal cavity at about 1800K and the front face at 300K. In order to address this issue, an optimized design of the front face was proposed and simulated: it reaches 77% of the ideal black-body absorption efficiency but it requires a specifically designed solar concentrating system.

Acknowledgements

This study was funded by the European Project Solhycarb (2006-2010, Contract SES-CT2006-19770). The authors wish to thank Olivier Prévost and Marc Garrabos for their technical support during the solar reactor manufacturing and operation.

Nomenclature:

- C_{pi} Specific heat of species i (J/mol.K, function of temperature)
- DNI Direct normal irradiation (W/m²)
- F Total molar flow-rate (mol/s) (gaseous phase)
- F_i Molar flow-rate of species i (mol/s)
- $F_{0,i}$ Inlet molar flow-rate of species i (mol/s)
- ΔH° Standard reaction enthalpy (J/mol)
- NL Normal Liter (at normal conditions: 101.325 kPa and 273.15 K)
- P Absolute pressure (Pa)
- P_0 Absolute pressure at the tube entrance (Pa)
- P_{solar} Solar power input (W)
- Q_0 Inlet gas flow rate (m³/s) (calculated with the conditions in the tubes provided in Table 1)
- R Universal gas constant (8.314 J/mol K)
- T Absolute temperature (K)
- T_0 Reference temperature (298 K)
- V_r Reactor volume (m³)
- X_{CH_4} Methane conversion
- Y_C Carbon yield

Y_{H_2} Hydrogen yield

y_i Mole fraction of species i at the exit

Greek letters:

σ Stephan Boltzmann constant ($5.67 \cdot 10^{-8} \text{ W} \cdot \text{m}^{-2} \cdot \text{K}^{-4}$)

τ Mean residence time calculated at the real tube temperature and pressure ($\frac{V_r}{Q_0}$ (s))

References

- [1] P.L. Spath, W.A. Amos, Using a concentrating solar reactor to produce hydrogen and carbon black via thermal decomposition of natural gas: feasibility and economics, *Journal of Solar Energy Engineering* 125 (2003) 159-164.
- [2] T. Pregger, D. Graf, W. Krewitt, C. Sattler, M. Roeb, S. Möller, Prospects of solar thermal hydrogen production processes, *International Journal of Hydrogen Energy* 34 (2009) 4256-4267.
- [3] F.C. Lockwood, J.E. Van Niekerk, Parametric Study of a Carbon Black Oil Furnace, *Combustion and Flame* 103 (1995) 76-90.
- [4] J.K. Dahl, K.J. Buechler, R. Finley, T. Stanislaus, A.W. Weimer, A. Lewandowski, C. Bingham, A. Smeets, A. Schneider, Rapid solar-thermal dissociation of natural gas in an aerosol flow reactor, *Energy* 29 (2004) 715-725.
- [5] J.B. Donnet, R.C. Bansal, M.J. Wang, *Carbon Black*, Second edition, Revised and expanded, Science and Technology, Marcel Dekker, New York, 1993.

- [6] N. Muradov, T.N. Veziroglu, "Green" path from fossil-based to hydrogen economy: An overview of carbon-neutral technologies, *International Journal of Hydrogen Energy* 33 (2008) 6804-6839.
- [7] G. Maag, G. Zanganeh, A. Steinfeld, Solar thermal cracking of methane in a particle-flow reactor for the co-production of hydrogen and carbon, *International Journal of Hydrogen Energy* 34 (2009) 7676-7685.
- [8] G. Maag, W. Lipinski, A. Steinfeld, Particle-gas reacting flow under concentrated solar irradiation, *International Journal of Heat and Mass Transfer* 52 (2009) 4997-5004.
- [9] M. Kogan, A. Kogan, Production of hydrogen and carbon by solar thermal methane splitting. I. The unseeded reactor, *International Journal of Hydrogen Energy* 28 (2003) 1187-1198.
- [10] A. Kogan, M. Kogan, S. Barak, Production of hydrogen and carbon by solar thermal methane splitting. III. Fluidization, entrainment and seeding powder particles into a volumetric solar receiver, *International Journal of Hydrogen Energy* 30(1) (2005) 35-43.
- [11] D. Hirsch, A. Steinfeld, Solar hydrogen production by thermal decomposition of natural gas using a vortex-flow reactor, *International Journal of Hydrogen Energy* 29(1) (2004) 47-55.
- [12] J.K. Dahl, K.J. Buechler, A.W. Weimer, A. Lewandowski and C. Bingham, Solar-thermal dissociation of methane in a fluid-wall aerosol flow reactor, *International Journal of Hydrogen Energy* 29 (2004) 725-736.
- [13] S. Rodat, S. Abanades, G. Flamant, High-Temperature Solar Methane Dissociation in a Multitubular Cavity-Type Reactor in the Temperature Range 1823-2073 K, *Energy & Fuels* 23 (2009) 2666-2674.

- [14] J.K. Dahl, V.H. Barocas, D.E. Clough, A.W. Weimer, Intrinsic kinetics for rapid decomposition of methane in an aerosol flow reactor, *International Journal of Hydrogen Energy* 27 (2002) 377-386.
- [15] S. Rodat, S. Abanades, J. Coulié, G. Flamant, Kinetic modelling of methane decomposition in a tubular solar reactor, *Chemical Engineering Journal* 146 (2009) 120-127.
- [16] M. Younessi-Sinaki, E.A. Matida, F. Hamdullahpur, Kinetic model of homogeneous thermal decomposition of methane and ethane, *International Journal of Hydrogen Energy* 34 (2009) 3710-3716.
- [17] N. Ozalp, A. Kogan, M. Epstein, Solar decomposition of fossil fuels as an option for sustainability, *International Journal of Hydrogen Energy* 34 (2009) 710-720.
- [18] H.F. Abbas, W.M.A. Wan Daud, Hydrogen production by methane decomposition: A review, *International Journal of Hydrogen Energy* 35 (2010) 1160-1190.
- [19] C. Caliot, S. Abanades, A. Soufiani, G. Flamant, Effects of non-gray thermal radiation on the heating of a methane laminar flow at high temperature, *Fuel* 88 (2009) 617-624.
- [20] A. Kogan, M. Israeli, E. Alcobi, Production of hydrogen and carbon by solar thermal methane splitting. IV. Preliminary simulation of a confined tornado flow configuration by computational fluid dynamics, *International Journal of Hydrogen Energy* 32 (2007) 4800-4810.
- [21] N. Ozalp, D. JayaKrishna, CFD analysis on the influence of helical carving in a vortex flow solar reactor, *International Journal of Hydrogen Energy* (2010) In Press.
- [22] S. Rodat, S. Abanades, J.L. Sans, G. Flamant, Hydrogen production from solar thermal dissociation of natural gas: development of a 10 kW solar chemical reactor prototype, *Solar Energy* 83 (2009) 1599-1610.

[23] D. Trommer, D. Hirsch, A. Steinfeld, Kinetic investigation of the thermal decomposition of CH₄ by direct irradiation of a vortex-flow laden with carbon particles, *International Journal of Hydrogen Energy* 29 (2004) 627-633.

[24] N. Muradov, F. Smith, A.T-Raissi, Catalytic activity of carbons for methane decomposition reaction, *Catalysis Today* 102-103 (2005) 225-233.

[25] A. Steinfeld, R. Palumbo, *Encyclopedia of physical science & technologie*, R.A. Meyers Ed., Academic Press. 15, 2001, pp. 237-256.

Figure captions:

Figure 1: Energy balance of the solar methane cracking

Figure 2: Schematic of the pilot-scale solar reactor

Figure 3: Global experimental flow-sheet of the solar reactor

Figure 4: Position of the temperature sensors

Figure 5: Experimental installation at the focus of the 1 MW solar furnace

Figure 6: Online monitoring of temperatures, DNI, H₂ and CH₄ off-gas mole fractions

Figure 7: CH₄ conversion, H₂ yield, and C yield versus temperature for the first experimental series (Ar: 31.5 NL/min, CH₄: 10.5 NL/min)

Figure 8: CH₄ conversion, H₂ yield, and C yield versus temperature for the second experimental series (CH₄: 21 NL/min)

Figure 9: Total power and mean flux density (measured at the cavity entrance) versus reactor temperature

Figure 10: Thermochemical and thermal efficiencies of the solar reactor

Figure 11: 2D axisymmetric mesh of the cavity solar receiver

Figure 12: Temperature of the cavity as a function of the heat sink for 28.4 kW of entering power at the cavity entrance (equivalent to 53 kW at the aperture)

Figure 13: Temperature profile (K) of the new design for 53 kW of entering power at the aperture and 35 kW heat sink